

## Inelastic electron scattering investigation of the Sb/GaAs(110) system

G. Annovi, Maria Grazia Betti,\* U. del Pennino, and Carlo Mariani

*Dipartimento di Fisica, Università degli Studi di Modena, via Campi 213/A, I-41100 Modena, Italy*

(Received 27 December 1989)

A high-resolution electron-energy-loss spectroscopy study of the Sb/[*n*-type GaAs (110)] system grown at room temperature is presented. A very wide range of antimony coverages was exploited (from 0.02 to 200 monolayers). The amorphous-polycrystalline transition accompanied by the semiconductor-metal transition, taking place in the deposited overlayer, was brought into evidence through the analysis of the energy-loss structures related to the electronic and the vibrational excitations of the system in different energy-loss regions. In particular, the intensity change and the energy shift undergone by the substrate's Fuchs-Kliever optical phonon, and the intensity modification of the dopant-induced free-carrier plasmon, marked a critical value for 15 monolayers coverage. The band-bending change upon antimony chemisorption has also been estimated from the plasmon-energy position, and an origin for the states inducing the Fermi-level pinning has been suggested. The evolution as a function of coverage of an electronic excitation proper of Sb, which shifts from 90 to 125 meV of loss energy, has been explained as being due to a "size effect" due to the varying overlayer thickness. This result has been obtained through the comparison of the experimental loss function with a model one. Moreover, the dielectric function of antimony has been determined in the 0.045–0.5-eV energy range. The high-resolution electron-energy-loss technique is also presented as a superb probe for the study of the electronic structure of narrow-band-gap surface and interface systems.

### I. INTRODUCTION

The study of the electronic and vibrational properties of group-V elements chemisorbed on polar III-V compound semiconductors has attracted much interest in the last decade. Among the most extensively studied interfaces, Sb/GaAs(110) can be considered a real model system of the epitaxial growth. Investigation of the reactivity, the kinetics of chemisorption and the growth morphology, the Schottky-barrier formation mechanisms, and the change in the electronic and vibrational structures, by deposition of Sb on GaAs(110), has been the subject of several works in recent years.<sup>1–22</sup> A large number of experimental<sup>1–4,8–22</sup> and theoretical<sup>5–7</sup> works were based mainly on electron-spectroscopy measurements and on band-structure calculations. They led to a picture of the Sb growth onto GaAs(110) at room temperature which we shall very briefly review. Antimony strongly bonds to the (110) surface of GaAs and, at submonolayer coverage, forms ordered clusters along the zig-zag chains of cations and anions in the [110] direction.<sup>21</sup> At the completion of 1 monolayer (ML), Sb atoms build up a structure with high chemical stability and local order, periodically arranged so as to resemble the geometry of a GaAs(110) topmost layer.<sup>3,4</sup> The stability is due to the establishment of strong covalent bonds between the overlayer atoms and the surface Ga and As atoms along the zig-zag chains. In order to obtain a large-scale ordered monolayer, a thermal treatment after deposition of a thicker layer is required.<sup>3,18</sup> At higher coverages, three-dimensional growth of Sb follows without interdiffusion into the substrate.<sup>3</sup>

While the submonolayer and monolayer coverage

ranges play a key role in the understanding of several physical phenomena occurring at the Sb/GaAs(110) interface, the higher coverages are of the greatest interest as well. At coverages higher than 1 ML, Sb grows as an amorphous structure that undergoes a transition to a polycrystalline atomic disposition at about 15 ML.<sup>13–16</sup> This transition is accompanied by a parallel modification of the dielectric properties of the overlayer, from semiconducting to semimetallic. This dielectric transition was brought into evidence on the basis of ellipsometric and photoemission measurements.<sup>13</sup> It was shown that the Sb overlayer deposited on GaAs(110) had semiconducting properties up to a coverage of 15 ML, while clear metallic character was present at larger thickness. On the other hand, the picture of the Sb-overlayer structure formation on GaAs(110) has been recently established through reflection high-energy electron-diffraction (RHEED) measurements.<sup>16</sup> They showed the disappearance of the typical substrate RHEED pattern (indicative of a random disposition of the overlayer atoms) for Sb thicknesses as high as 20 ML. At this coverage the diffraction pattern suddenly reappeared, showing a structure due to Sb crystallites all oriented with the basal crystalline plane in contact with the substrate and with random azimuth. The same structural evidence of a crystallization of the overlayer—at a coverage of 12 ML—was previously deduced from analysis of Raman-effect measurements on the same interface system.<sup>14,15</sup> In those experiments the appearance of two distinct phonon peaks, characteristic of crystalline antimony<sup>23,24</sup> and clearly different from broader structures found in amorphous Sb,<sup>25</sup> marked the structural transition. Moreover, band-bending changes at the interface have been observed even

after deposition of tens of monolayers.<sup>14</sup>

Thus, the transition from a semiconducting to a metallic state in the Sb overlayer deposited onto GaAs(110) was first experimentally established at about 15 ML of coverage. Then the amorphous-polycrystalline transition taking place in the overlayer was brought into evidence, and interpreted as being responsible for the dielectric transition. This assumption is reasonable, since in a very early work by Moss<sup>26</sup> the semiconducting character of amorphous Sb and As had been established. Furthermore, the valence-band densities of states of Sb, As, and Bi have been measured for their respective crystalline and amorphous phases,<sup>27</sup> showing the different densities of occupied states. Other works on the optical properties of amorphous<sup>28–30</sup> and crystalline<sup>31</sup> arsenic again highlight the relationship between the structural and electronic properties of group-V elements.

Hence, the characterization of the Sb/GaAs(110) system at higher coverages must be considered fundamental for better understanding of the physical processes underlying the structural and dielectric transitions of the overlayer at completion of about 15 ML. Nevertheless—as far as we know—only the works quoted above<sup>13–16</sup> dealt with the case of Sb coverages up to a few tens of ML. Therefore, we decided to study in detail the electronic and vibrational properties of the Sb/GaAs(110) system in a wide coverage and energy range by means of the energy-loss technique.

The high-resolution electron-energy-loss spectroscopy (HREELS) technique is particularly suitable for studying surface, interface, and ultrathin-film systems in III-V compound semiconductors. In fact, when used in the specular direction geometry (i.e., interpretable in the dipolar scattering approximation<sup>32</sup>), HREELS has a probing depth “tunable” along the direction normal to the crystal surface ( $z$ ), through the modification of the kinematic conditions of the experiment. The HREELS technique has been extensively used to characterize the vibrational and electronic structure of the clean  $n$ -type-doped GaAs(110) surface.<sup>33–36</sup> In particular, a correlation between the energy position of the dopant-free-carrier-induced plasmon and the space-charge layer below the surface was revealed.<sup>34,36</sup> Indeed, we shall deduce the properties of Sb/GaAs(110) from the modifications of the Fuchs-Kliever optical phonon and of the plasmon. Moreover, the constant high energetic resolution in a wide energy range renders HREELS most suited for the study of the electronic properties of narrow-gap systems. It has been used, for example, to analyze the azimuthal dependence of the electronic excitations across the surface gap at about 0.45 eV, in the clean Si(111)-(2×1) reconstructed surface.<sup>37</sup> It also allowed the identification of a new structure in the energy-loss spectrum of the Sb/GaAs(110) system,<sup>38</sup> related to the narrow gap of antimony, which we will analyze in detail in this paper. Thus, HREELS is a very powerful surface technique for obtaining a complete picture of an interface system, using different kinematic conditions, chosen in such a way as to maximize the electron cross section of the several excitations (phonons, plasmons, interband transitions) under investigation.

We investigated the Sb/[ $n$ -type GaAs(110)] system within the framework described above. The overlayer was grown at room temperature and in a very wide coverage range (from 0.02 to 200 ML). The HREELS technique was used in a wide energy-loss range (0–1400 meV), focusing attention on the different spectral structures appearing in their relative energy regions. Much of the experimental evidence (energy and intensity variation of the phonon, change of the plasmon intensity, and modification of the elastic-peak width) was related to screening effects occurring in the system as the Sb coverage approached 15 ML. Thus, new information was added to the knowledge of the dielectric transition occurring in the overlayer. The plasmon position was related to the band bending occurring at the interface. The evolution of the loss structure due to the electronic transitions, upon increasing the coverage, was explained by comparison with the calculated model energy-loss function and ascribed to “size effects” due to increasing overlayer thickness. No other structure was detectable in the energy-loss spectrum up to the bulk band-gap energy of GaAs.

The paper is organized as follows. After a description of the experimental apparatus and of the characterization of antimony deposition, we describe the studied energy-loss regions and the relative experimental conditions. In the following section we first show the analysis of the elastic peak, the Fuchs-Kliever phonon, and the plasmon structures, all as functions of Sb coverage, and then we describe a structure related to an electronic transition proper of antimony. Then, a model loss function is calculated and discussed, along with comparison to the experimental loss function derived from the spectra.

## II. EXPERIMENT

### A. Experimental apparatus

The experiments were carried out in the surface-physics laboratory Laboratorio di Spettroscopia Elettronica di Superfici e Adsorbati, Modena (SESAMO), at the Dipartimento di Fisica, Università degli Studi di Modena. The ultrahigh-vacuum (UHV) system consisted of two experimental chambers separated by an all-metal valve and connected through a shiftable sample manipulator. The preparation chamber contained all the ancillary equipment for crystal cleaning, metal deposition, and characterization, while the measurement chamber was equipped with the HREELS spectrometer (double-pass monochromator-analyzer, Leybold Heraeus model ELS-22), a low-energy electron-diffraction (LEED) apparatus, and an x-ray photoemission spectroscopy (XPS) system with a double-pass cylindrical mirror electron analyzer. The pressure was kept always below  $7 \times 10^{-11}$  mbar ( $6.8 \times 10^{-9}$  Pa), except during Sb deposition, when it rose to  $2 \times 10^{-10}$  mbar. The vacuum was obtained by a combination of a turbomolecular magnetically suspended pump, a Ti-sublimation liquid-nitrogen-cooled pump, and a bakable He-cooled cryopump. Thus, the residual atmosphere was particularly free of organic contaminants.

The GaAs(110) single crystals were obtained from MCP Electronic Materials, Ltd. We used two differently *n*-type (Si) -doped sets of sets of specimens, one with a dopant concentration in the low- $10^{17}$ - $\text{cm}^{-3}$  range, the other with  $n = 4.0 \times 10^{18} \text{ cm}^{-3}$ . The clean surfaces were prepared by cleavage *in situ* by means of the single-wedge technique. After every good cleave, the cleaved faces appeared mirrorlike and exhibited large terraces of flat surfaces. They exhibited a perfect crystalline order, as shown by the very sharp LEED pattern. A lower number of good cleaves was obtained with the set of more-doped samples. The cleanliness of the surfaces was checked with XPS and with the energy-loss spectrum itself.

A computer-assisted data-acquisition system allowed careful calibration of the energy ramp before each HREELS spectrum, and we took the data in the energy-loss and gain regions, relative to the observed structures. Hence, we estimated an energy-loss accuracy of  $\pm 1 \text{ meV}$ .

### B. Preparation and characterization of the deposited Sb layers

Antimony deposition onto GaAs was obtained by sublimation of small Sb shots (99.999% purity) contained in a resistively heated quartz crucible. Sublimation rates depended on the desired coverage step and ranged between 0.1 and 10 ML/min. One monolayer of deposited Sb was defined as a density of atoms per unit surface equal to that of the substrate ( $0.88 \times 10^{15} \text{ atoms/cm}^2$ ). Thickness was determined by using a Sloan crystal-thickness monitor and independently by means of an XPS analysis of the Sb 3*d*, Sb 4*d*, Ga 3*d*, and As 3*d* core levels. A run of measurements was dedicated to the coverage calibration of the quartz balance through XPS. This was done by

measuring the XPS peak areas and by comparing them with previous synchrotron-radiation photoemission data of Skeath *et al.*,<sup>1</sup> accounting for the different probing depths and core-line-excitation cross sections<sup>39</sup> of our experiment. As an example, we show in Fig. 1 the intensity behavior of the Sb 4*d*, As 3*d*, and Ga 3*d* XPS peaks as a function of coverage. We chose these core levels since they lie close in energy and the analyzed photoelectrons come from a comparable probed depth. An exponential decrease of the substrate's related peaks and an uptake of the overlayer's peak intensity are present, upon increasing Sb coverage. This behavior indicates a continuous growth of the overlayer, within the experimental accuracy of our XPS data. Previous works,<sup>2,9,17,20</sup> mainly focused on the growth morphology of the first monolayers of Sb on GaAs(110), showed a slightly different behavior of the intensity of the Auger- and photoemission-related peaks versus coverage. A change in the slope of the curves describing the substrate-peak attenuation was put into evidence, at the completion of 1 ML. This effect has been attributed to three-dimensional growth of clusters on top of a uniform monolayer. We cannot exclude the fact that a similar change in the slope of the attenuation curves is also present in our data. Nevertheless, since we were interested in the physical phenomena subtending the growth of ultrathin layers of Sb on GaAs(110), our XPS analysis was performed only to obtain a reproducible calibration for the coverage estimation.

As it concerns the structural aspect of the growth, the  $(1 \times 1)$  LEED pattern was structurally unaffected up to a coverage of about 15 ML, although the spots were superimposed on a growing structureless background. No superstructure was detected. At higher coverages the LEED pattern disappeared, buried in the background. This behavior confirmed the epitaxial growth of the first

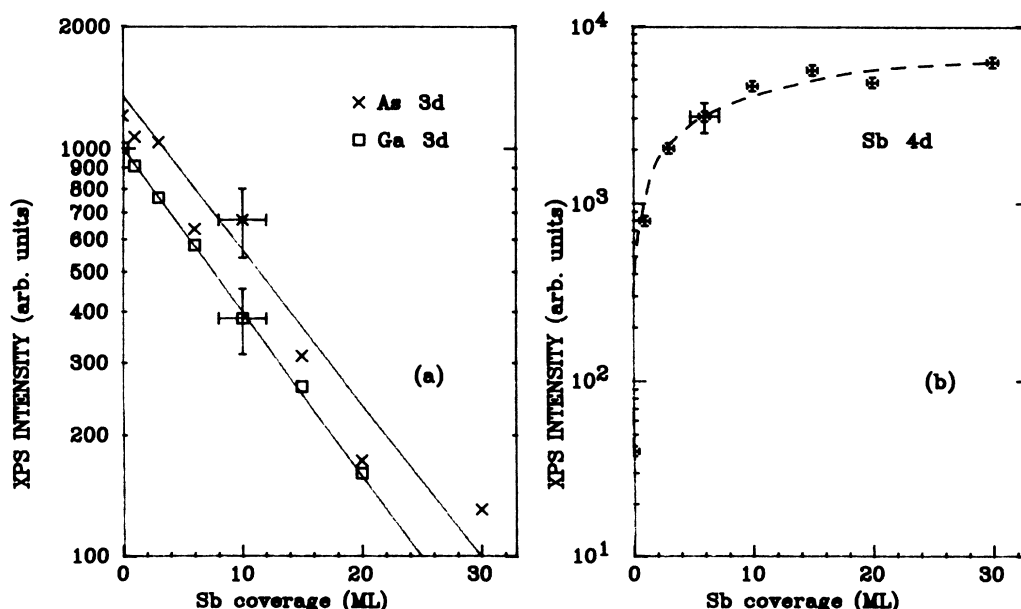


FIG. 1. (a) XPS intensity of the As and Ga 3*d* core levels as a function of the Sb coverage; (b) XPS intensity of the Sb 4*d* core level as a function of the Sb coverage.

monolayer as well as the absence of long-range order within the overlayer for coverages higher than 15 ML, in agreement with previous LEED data.<sup>2</sup>

### C. Energy-loss regions and kinematic conditions

All HREELS data was taken in specular geometry, with an angle of incidence of  $65^\circ$ , equal to the collecting angle. The energy resolution, evaluated as the full width at half maximum (FWHM) of the direct electron beam (i.e., of the elastic peak going straight from the electron monochromator into the analyzer, without reflection on the surface), was better than 8 meV. After reflection on the clean cleaved surface of GaAs, the energy resolution reached about 10–12 meV, depending on the experimental conditions.

We performed a few series of three different sets of HREELS measurements. Each set was taken on GaAs crystals with a suitable choice of doping level and/or kinematic conditions ( $E_p$  values) to enhance the scattering cross section of the excitations under examination. A first set of measurements was taken to study the GaAs Fuchs-Kliever optical phonon and the elastic peak. We used the less-doped samples and  $E_p = 4.7$  eV in order to have the plasmon at low energy loss and with low intensity.<sup>34</sup> The second set of measurements focused on the dopant-induced free-carrier-induced plasmon. We used, therefore, the more-doped samples (leading to a plasmon frequency of about 77 meV) and  $E_p = 20$  eV, to achieve a high excitation cross section for this loss structure.<sup>34</sup> The last set of data was taken on the lower-doped samples and with  $E_p = 20$  eV, to obtain a low-frequency plasmon and a low-intensity phonon, and to enhance the low-energy electronic transitions.

## III. RESULTS AND DISCUSSION

### A. Elastic-peak energy region

The spectra taken in the first set of measurements (low doping level,  $E_p = 4.7$  eV), centered on the elastic-peak structure, are shown in Fig. 2, as a function of the Sb coverage. Spectra were normalized to the peak height. In addition to the main structure due to the elastic peak, the feature at about 34.5 meV is due to the excitation of the surface optical phonon of GaAs. The elastic-peak width first increases, and then, from a certain coverage value, starts narrowing. In order to get a quantitative evaluation of the peak intensity and width, we fitted the data with Gaussian curves corresponding to the elastic peak and the Fuchs-Kliever phonon. The results of this procedure are shown in Figs. 3 and 4, where the elastic-peak intensity (peak height) and width (FWHM) are plotted. The error bar we quote in the figures is not due to the fit (it would be much lower); it was derived from the reproducibility of the spectra in different series of measurements.

The elastic-peak intensity shows a reduction, with respect to the clean-surface data, as 1 ML of Sb is deposited (Fig. 3), while at this coverage the LEED pattern still showed the  $(1 \times 1)$  substrate structure. A further step of

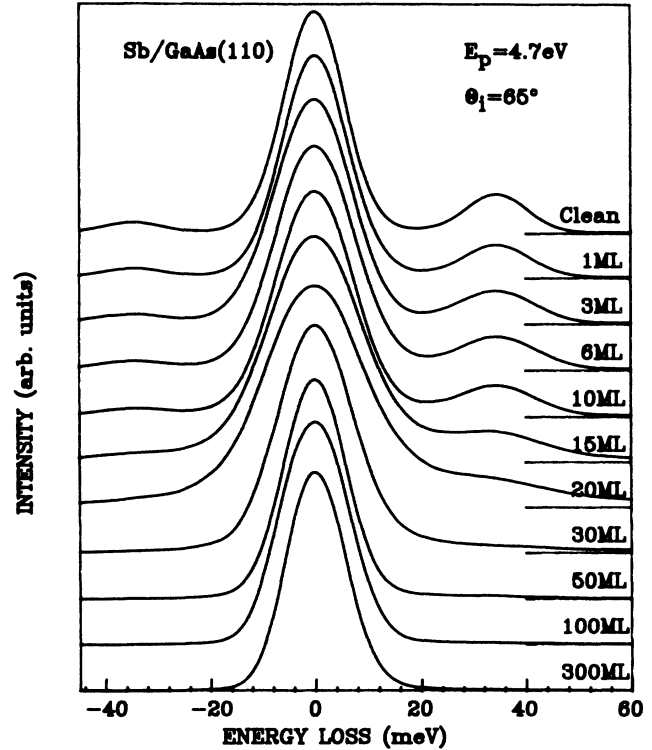


FIG. 2. High-resolution electron-energy-loss spectra of the Sb/[*n*-type GaAs(110)] system, as a function of the Sb coverage, in the elastic-peak-energy region. Primary beam energy  $E_p = 4.7$  eV; angle of incidence  $\theta_i \approx 65^\circ$ ; doping concentration  $n \sim 10^{17} \text{ cm}^{-3}$ . Spectra are normalized to the peak height.

intensity reduction is observed for a coverage  $\Theta > 4$  ML, and a diffused background grew onto the  $(1 \times 1)$  LEED spots at this stage of coverage. At  $\Theta \approx 15$  ML we observe a major lowering of intensity, while the LEED pattern disappeared, buried in the diffused background. The changes of the elastic-peak intensity reflect the modifications of the LEED image. In fact, as antimony builds up a uniform monolayer by coalescence of large

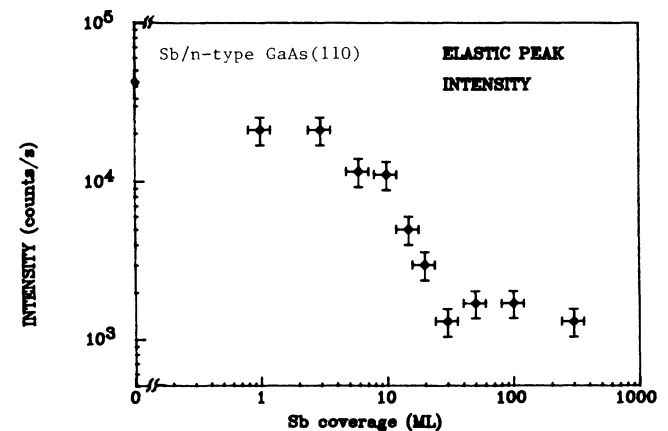


FIG. 3. Elastic-peak intensity as a function of the Sb coverage.

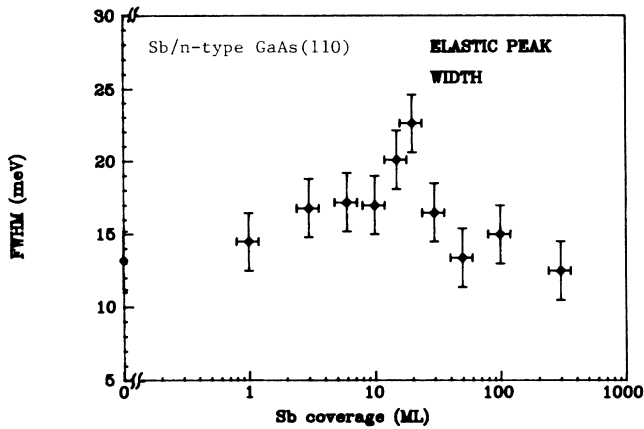


FIG. 4. Elastic-peak width as a function of the Sb coverage.

terraces formed in the submonolayer coverage,<sup>21</sup> a different reflectivity of the surface is observed. An amorphous phase follows from the ordered one, and the layer becomes polycrystalline in the 4–15-ML coverage range. All these complex structural modifications lead to changes of the reflectivity of the surface, which we identify through the intensity variations of the elastic peak in the respective structural phases.

As far as the elastic-peak width is concerned (Fig. 4), a continuous increase is observed (from 13 to about 23 meV), up to a coverage of 20 ML. Then it narrows for higher coverages, reaching 12 meV, the same value obtained for a thick Sb layer (not shown in the figures). The surface atomic disorder cannot be the only cause of the broadening, since it would lead to a symmetric shape, while an asymmetric peak with a tail on the energy-loss side of the spectra is observed. Actually, the elastic-peak structure is the convolution of the peak due to the back-scattered electrons that have not undergone any loss of energy, with the features due to the very-low-energy-loss excitations. We speak in terms of an elastic peak only for the sake of simplicity, this structure being more properly termed a quasielastic peak. Thus, the broadening of the elastic peak must be related to the presence of features at a few meV of energy, whose intensity increases upon antimony deposition, up to the critical coverage of 15–20 ML. We can also exclude as the cause of the broadening the presence of the dopant-induced free-carrier plasmon. In fact, although it had an energy of about 20 meV, the kinematic conditions we chose for this set of data were unfavorable for its excitation. On the other hand, in different measurements taken on the same sample and in conditions able to enhance the plasmon intensity, the evaluation of the elastic-peak width confirmed the data presented here, even if with lower sensitivity (see Fig. 2 in Ref. 38).

Similar behavior of the elastic-peak width was observed in the Ag/GaAs(100) interface by Dubois *et al.*,<sup>40</sup> as the overlayer thickness increased. A continuous peak broadening was measured, up to the formation of a 2.5-Å-thick silver film, followed by a narrowing at higher coverages. A layer model (vacuum-overlayer-substrate) (Ref. 32) was used to fit the experimental data and to ex-

plain the observed effects. Although in our system the critical coverage for the inversion of the elastic-peak broadening (15 ML) is different from that found by Dubois *et al.*,<sup>40</sup> a close similarity exists in the two experiments. On the other hand, antimony is semimetallic, while silver is a pure metal. Following their interpretation of the phenomenon, we explain the broadening and subsequent narrowing of the quasielastic peak (as the Sb coverage increases) as being due to an interaction between the overlayer excitations and the substrate's phonon excitation. As a thickness is reached for which the phonon peak is no longer detected, the overlayer screens the electric field produced by the substrate's surface vibrations, leading to a narrower elastic peak.

In conclusion, from the analysis of the intensity and of the width of the elastic peak—as a function of Sb coverage—a critical value  $\Theta \approx 15\text{--}20$  ML is determined at which the system's properties switch from semiconducting to metallic. This coverage value will be found to be critical for every physical characteristic of the energy-loss structures we will show in the following sections.

### B. Fuchs-Kliwer phonon-energy region

The measurements performed to study the behavior of the GaAs surface optical phonon as a function of Sb coverage were taken at  $E_p = 4.7$  eV to enhance the phonon-excitation cross section and on the less-doped crystal to ensure a relatively low plasmon frequency.<sup>34</sup> As a matter of fact, the phonon peak is due to a higher mode of a phonon-plasmon-coupled excitation, superimposed on the unscreened longitudinal-optical phonon of GaAs.<sup>41</sup> However, due to the low doping level ( $n \approx 10^{17}$  cm<sup>-3</sup>), we can assume the lower-energy mode to be highly plasmon-like in character, can assume the higher-energy branch to be phononlike,<sup>34</sup> and can consider the structure a pure vibrational mode.

Spectra are shown in Fig. 5. The Fuchs-Kliwer phonon loss is at about 34.5 meV (for the clean surface); the corresponding gain structure at  $-34.5$  meV and the double-loss replica at 69 meV can also be observed. It is already noticeable from Fig. 5 that phonon intensity and position change as Sb coverage approaches a value of about 15 ML. In order to get a quantitative estimation, we performed a fit of the data, by assuming all the structures to have a Gaussian shape. Although Lorentzian curves would, in principle, better describe the losses, we found that use of Gaussians enabled a good fit to the spectra, as the experimental energy resolution is the main broadening factor. We chose four independent Gaussian curves, reproducing the elastic peak, the plasmon loss, the Fuchs-Kliwer phonon, and the latter's double-loss structure, respectively. The four curves were allowed to vary independently. We also considered the respective gain peaks, by assuming a Boltzmann factor for their relative intensities. As an example, we show in Fig. 6 the analysis for the clean GaAs surface and a Sb coverage of 6 ML. The experimental data are plotted together with the resulting fit curves, while only the Gaussians relative to the elastic peak, the plasmon, and the phonon are shown. From the fit procedure we deduce a plasmon en-

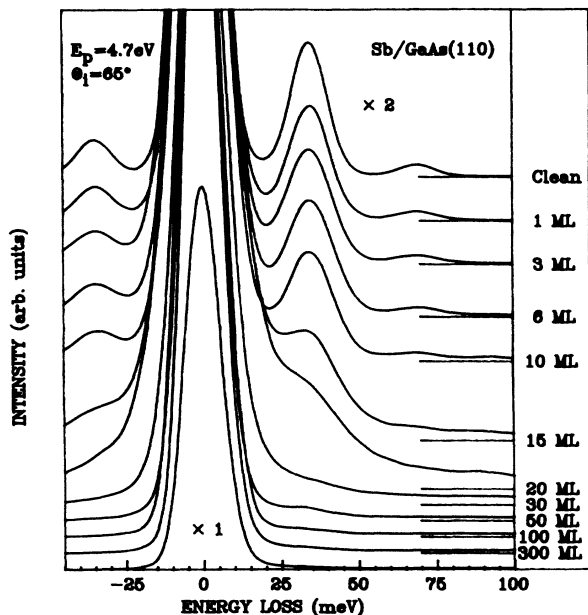


FIG. 5. High-resolution electron-energy-loss spectra of the Sb/[*n*-type GaAs(110)] system, as a function of the Sb coverage, in the Fuchs-Kliwer optical-phonon-energy region. Primary beam energy  $E_p = 4.7$  eV; angle of incidence  $\theta_i \approx 65^\circ$ ; doping concentration  $n \sim 10^{17} \text{ cm}^{-3}$ . Spectra are normalized to the respective elastic peak heights.

ergy between 20 and 24 meV, a reasonable value for the actual doping level. We also verified that the intensity attenuation for the phonon double-loss replica was Poissonian, with respect to the excitation of the single loss. The intensity of the Fuchs-Kliwer phonon (given by the peak area normalized to that of the elastic peak) is shown

in Fig. 7, as a function of coverage. The energy positions of the phonon loss and of its double-loss replica are plotted in Fig. 8.

Upon increasing the overlayer thickness, the phonon intensity (Fig. 7) shows a clear attenuation, starting from the lower values of the coverage  $\Theta$ , with a behavior corresponding to a  $\Theta^{-\alpha}$  law. At  $\Theta \approx 20$  ML the attenuation rate increases, leading to a curve with a higher slope. In correspondence with this critical coverage, the  $\alpha$  value changes from 0.1 to 1.4. We ascribe the low-rate intensity reduction—seen in the first part of the plot—to a continuous increase of the overlayer thickness. The sudden uptake of the attenuation rate is indicative of increased dielectric screening. Thus, the critical coverage of 20 ML marks the modification of the dielectric structure of the Sb overlayer, showing that the transition from a semiconducting to a more metallic state is completed.

The Fuchs-Kliwer phonon-energy-loss value ( $34.5 \pm 1.0$  meV) does not change as the first monolayers of antimony are deposited onto GaAs (Fig. 8). At  $\Theta \approx 10$  ML the phonon changes its frequency slightly, ending up at  $28.5 \pm 1.0$  meV for  $\Theta \approx 20$  ML, and then maintains this value as far as the structure is still detectable. The energy shift (6 meV) is reproduced very well by the corresponding double shift of the double-loss replica (12 meV). Since these results come from independent curve fitting, we measured without a doubt a frequency modification of the phonon at the higher Sb coverages. The phonon energy is not affected by the deposition of the first Sb layers. Therefore, we think that the effect might be related to the crystallization occurring in the overlayer.

The change of dielectric screening and the structural modifications in the overlayer we invoked to explain the behavior of the intensity and position of the phonon at a coverage of about 15 ML can be indirectly confirmed by previous studies of arsenic.<sup>28,30</sup> In fact, in these works

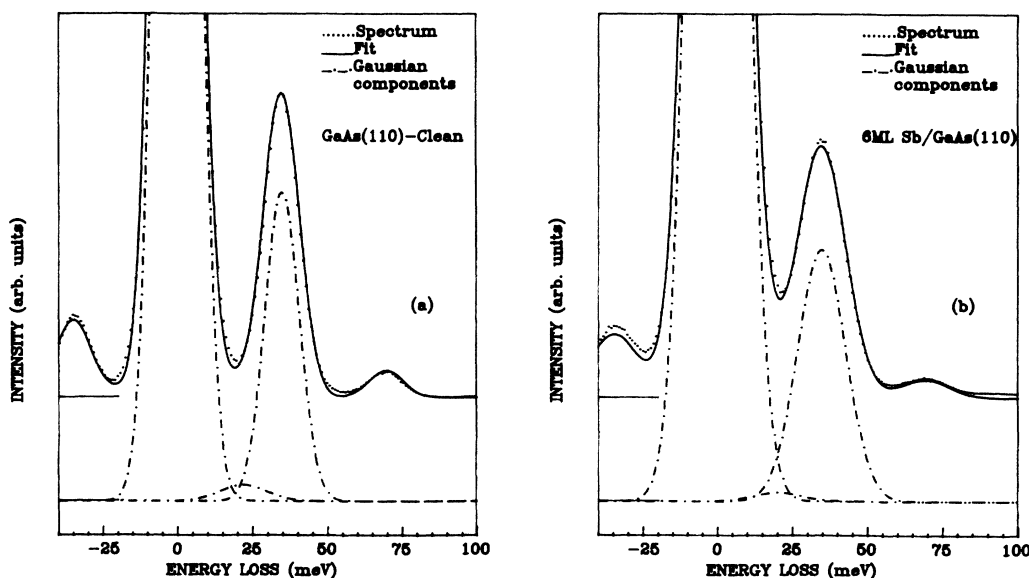


FIG. 6. Fit of two of the spectra appearing in Fig. 5: those corresponding to (a) the clean surface and (b) to the coverage of 6 ML. Each experimental data (dotted line) is shown together with the fit curve (solid line). The Gaussian components relative to the elastic peak, the phonon, and the plasmon (dashed-dotted lines) are shifted along the vertical axis, for clarity.

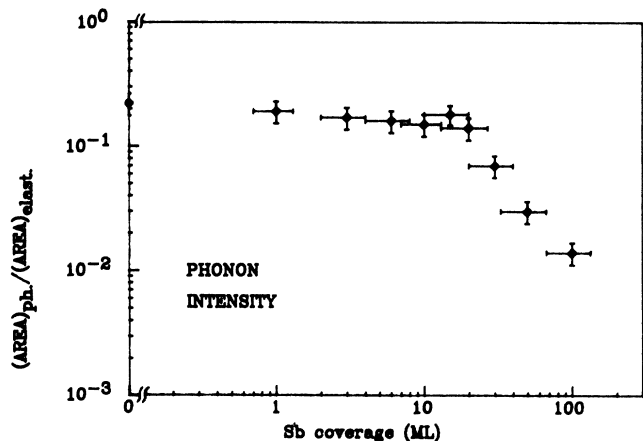


FIG. 7. Fuchs-Kliewer phonon intensity as a function of the Sb coverage.

the dielectric functions of both the amorphous and crystalline phases of As were derived at very low energy. A complex dielectric function typical of a semiconductor was found for the amorphous structure, while metallic behavior resulted for crystalline As.

Another symptom of the crystallization of an antimony overlayer deposited onto GaAs(110) was the appearance of two typical vibrational structures of crystalline Sb (Refs. 23 and 24) in the Raman spectra of the Sb/GaAs(110) interface at  $\Theta \approx 12\text{--}15$  ML.<sup>14,15</sup> We cannot rule out the possibility that the energy shift of the Fuchs-Kliewer phonon is related to the coupling with those vibrational structures of Sb, when it crystallizes; therefore, theoretical work on this argument is welcome.

Looking carefully at the critical coverages appearing in Figs. 7 and 8, we see how the intensity slope (versus coverage) changes at  $\Theta = 20$  ML, while the phonon loss energy starts to change at  $\Theta = 10$  ML. Thus, the frequency of

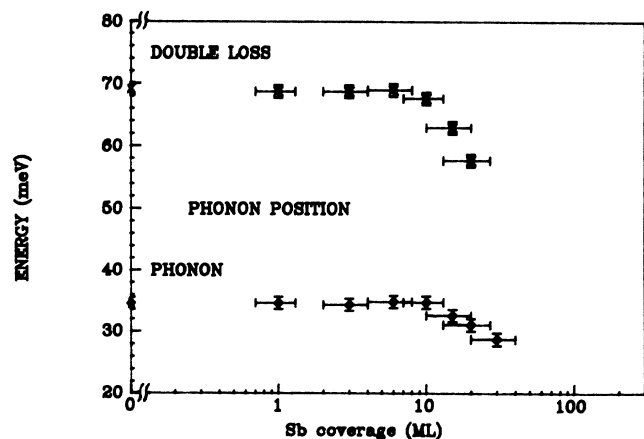


FIG. 8. Energy position of the Fuchs-Kliewer phonon loss structure (lower curve) and of its double-loss replica (higher curve), as a function of the Sb coverage.

this vibrational mode changes when the layer is 10 ML thick, while its intensity maintains the same attenuation rate it has at the lower coverages. A possible explanation for these different values of the critical coverage (beyond the experimental errors) could be found by making some hypotheses on the crystallization mechanism. If we suppose that Sb starts the crystallization at the Sb/GaAs interface for  $\Theta = 10$  ML, then the Fuchs-Kliewer phonon would be influenced by the crystal structure close to the substrate, modifying its energy. If we assume that a complete crystallization of the full layer stops only when 20 ML are completed, then the metallic dielectric screening affects the phonon intensity only when the overlayer is fully crystalline. However, we think that this effect demonstrates the complex crystallization dynamics of the overlayer.

### C. Plasmon-energy region

The plasmon due to the excitation of the conduction-band free carriers given by the dopants in *n*-type GaAs has been extensively and carefully analyzed theoretically<sup>36,41,42</sup> and experimentally by means of HREELS,<sup>34,43</sup> among other techniques. For the clean substrate the plasmon frequency is a function of the surface-charge-layer thickness. In fact, the free-carrier density varies dramatically near the surface. When there is neither surface contamination or defects that could induce a depletion layer, a surface-charge region still exists due to the boundary condition between the vacuum and the solid. This layer has been formerly defined as a “dead layer,” a thin region close to the surface where the charge density drops to zero.<sup>36,42</sup> In a previous HREELS work by Betti *et al.*,<sup>34</sup> the plasmon measured on the clean GaAs(110) surface, in the absence of a depletion layer, was confirmed to be a “subsurface” mode by studying its excitation cross section as a function of the primary beam energy (i.e., of the probing depth). Matz and Lüth,<sup>33</sup> and more recently Chen *et al.*<sup>43</sup> observed how the plasmon shifts in energy when the depletion-layer thickness is increased, by chemisorbing hydrogen on *n*-type GaAs. Chen *et al.*<sup>43</sup> also calculated a relation between the depletion-layer thickness and the plasmon loss energy, for a crystal with a bulk doping concentration  $n = 4.0 \times 10^{18} \text{ cm}^{-3}$ . The depletion-layer thickness—the consequence of band bending at the *n*-type GaAs(110) surface—is very sensitive to (a) structural defects at the surface, and (b) surface contamination. Both effects induce states on the surface which lead to a band bending and to the formation of a depletion layer. (a) On different cleaves of the same high-doped crystals ( $n = 4 \times 10^{18} \text{ cm}^{-3}$ ), we measured different plasmon energies as a function of the cleavage quality, i.e., of the concentration of defects per unit surface area. We also noticed that this high rate of nonperfect cleaves was reduced when crystals with lower dopant concentration were used. (b) On the good cleaved surfaces of the more-doped samples, we measured a noticeable change of the plasmon energy as a function of the elapsed time after cleavage, in agreement with that observed by Chen *et al.*<sup>43</sup> In fact, a plasmon peak at about 77 meV shifted to 65 meV after about 10 h of expo-

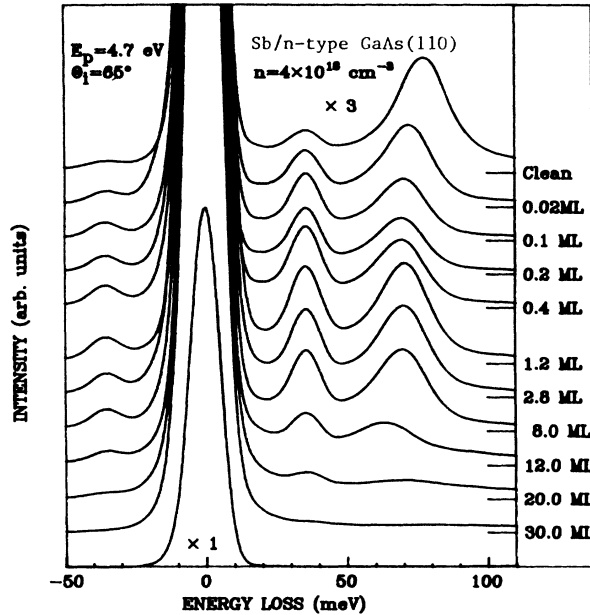


FIG. 9. High-resolution electron-energy-loss spectra of the Sb/[*n*-type GaAs(110)] system, as a function of the Sb coverage, in the energy region of the dopant-free-carrier-induced plasmon. Primary beam energy  $E_p = 20$  eV; angle of incidence  $\theta_i \approx 65^\circ$ ; doping concentration  $n = 4.0 \times 10^{18} \text{ cm}^{-3}$ . Spectra are normalized to the respective elastic-peak heights.

sition to the residual-gas atmosphere at a pressure of  $7 \times 10^{-11}$  mbar, and under electron irradiation with a beam current of less than 1 nA. Hence, the study of the dopant-free-carrier-induced plasmon can be extremely useful for an estimation of the band bending and of the depletion layer in a metal-semiconductor system.

For the measurements relative to the Sb/[*n*-type GaAs(110)] system, we exploited the more-doped sample, so as to have the plasmon and the phonon losses well distinguished in terms of energy from each other. The HREELS data are shown in Fig. 9. The spectrum relative to the clean surface was taken within 15 min after cleavage, to minimize the contamination effects. The structure at about 35 meV is due to the Fuchs-Kliwer phonon, while the intense loss at  $77.5 \pm 1.0$  meV is due to plasmon excitation. The phonon double-loss replica (at about 69 meV) is hidden below the plasmon peak, but it does not significantly affect this loss, since its intensity is negligible (given the chosen kinematic conditions). We deposited antimony in small steps of coverage, starting from a few hundredths of ML, since it is well known that such low depositions can already affect the space-charge layer at the surface. The plasmon intensity and energy position changed as the Sb coverage increased. The plasmon loss was no longer detectable at  $\Theta \approx 30$  ML. We analyzed the data with the same fitting procedure used for the sets of measurements relative to the phonon, using Gaussian curves. The results of this analysis are shown in Fig. 10 for the plasmon intensity (normalized to the elastic-peak intensity) and in Fig. 11 for the plasmon fre-

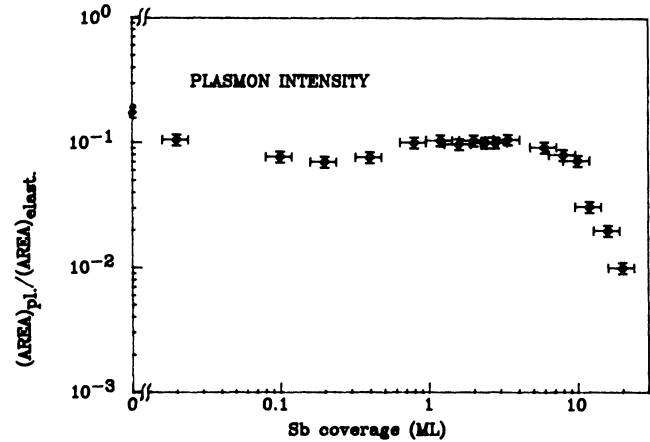


FIG. 10. Plasmon intensity as a function of the Sb coverage.

quency.

The plasmon-peak intensity (Fig. 10) already shows a decrease at  $\Theta \approx 0.02$  ML and a relative minimum at  $\Theta \approx 0.2$  ML, followed by a small increase and by a flat region, for coverages between 0.7 and 8 ML. The small variations of the intensity in the coverage range 0–8 ML may be due to the combination between the shift of the localization of the maximum of the plasmon wave function towards deeper depths normal to the surface and the increasing overlayer thickness. A stronger intensity reduction takes place at  $\Theta \approx 15$  ML. At this coverage, the effect due to the depletion layer and the subsurface localization of the plasmon is overwhelmed by screening effects. In fact, as in the case of the phonon intensity, we attribute this intensity decrease to a modification of the screening properties of the overlayer, a consequence of the crystallization of antimony.

The frequency of the measured plasmon (Fig. 11) decreases from  $77.5 \pm 1.0$  to 70 meV, as only 0.02 ML of antimony is deposited. It varies within 2–3 meV for cover-

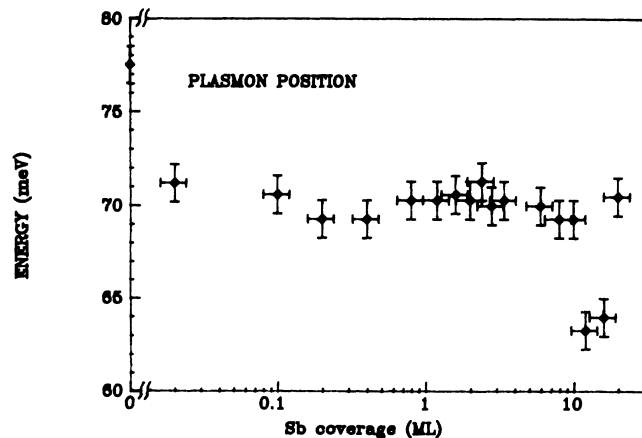


FIG. 11. Energy position of the plasmon as a function of the Sb coverage.

ages between 0.02 and 8 ML. It drops to 64 meV at  $\Theta \approx 10$  ML and rises again to 70.5 meV at  $\Theta \approx 20$  ML. Following the model by Chen *et al.*<sup>43</sup> briefly described above, the plasmon energy that we measured on the clean surface corresponds to a space-charge-layer thickness of about 40 Å, for a GaAs crystal with the given doping level. This is a reasonable value, corresponding to a band bending of about 0.046 meV. As only 0.02 ML of Sb are deposited, we can estimate that the depletion-layer thickness is increased to about 160 Å and the band bending to 0.73 eV, values that remain for coverages up to 8 ML. Our estimation of the band-bending effect, derived from a measure of the plasmon loss energy, for the first monolayer of Sb at the interface with GaAs(110), is in very good agreement with previous experimental works.<sup>8,14,20</sup> In the submonolayer region the pinning of the Fermi level has been attributed to states localized at the edge of the Sb terraces on GaAs, as measured through scanning tunnelling microscopy.<sup>21</sup> The pinning was associated with unsaturated dangling bonds that are present when the monolayer is not yet completed, but that could be also present at higher coverage if the disorder still exists.<sup>22</sup> The theoretical studies of this interface showed that, for a zig-zag-chain model of chemisorption, an ordered full monolayer of Sb chemisorbed on GaAs(110) does not induce states within the semiconductor band gap.<sup>5,7</sup> This has also been confirmed experimentally.<sup>12,19</sup> Thus, the band bending for the ordered monolayer cannot be induced by the electronic interface states, but can be induced by other interface states of different nature. In agreement with the findings of Cao *et al.*,<sup>20</sup> we think that the band bending we deduce for coverages between 1 and 15 ML could be related to intrinsic states of GaAs. These intrinsic states may be associated to defects of the GaAs surface, formed during the Sb chemisorption.<sup>20</sup> Moreover, we detected no other states within the GaAs band gap, at coverages of 1.2 and 12 ML. The overlayer is not yet metallic in character at these stages of coverage, so that even gap states characteristic of the metal cannot be invoked to explain the band bending.

As the coverage approaches the critical coverage of 15 ML, the sudden decrease of the plasmon-energy loss would suggest a further increase in the space-charge-layer thickness. An estimation of the Fermi-level pinning subsequent to the deposition of several ML of antimony was deduced from the Raman-effect measurements performed by Pletschen *et al.*<sup>14</sup> A direct comparison with our estimation is not possible, since the band-bending behavior versus coverage is a strong function of the doping level and the crystal we used had a much higher concentration of dopant atoms. However, we observed probable modifications of the band-bending dynamics around the critical coverage of 15 ML, as Pletschen *et al.*<sup>14</sup> also did. The situation at this stage of coverage—and for such high doping levels—is really intriguing. The modifications of the plasmon energy might also be related to the appearance of an overlayer plasmon developing in the film. As a matter of fact, as we shall see in the next section, at  $\Theta \approx 15$  ML an excitation due to states proper of metallic Sb appeared in the HREELS spectra at about 0.1 eV of loss energy.

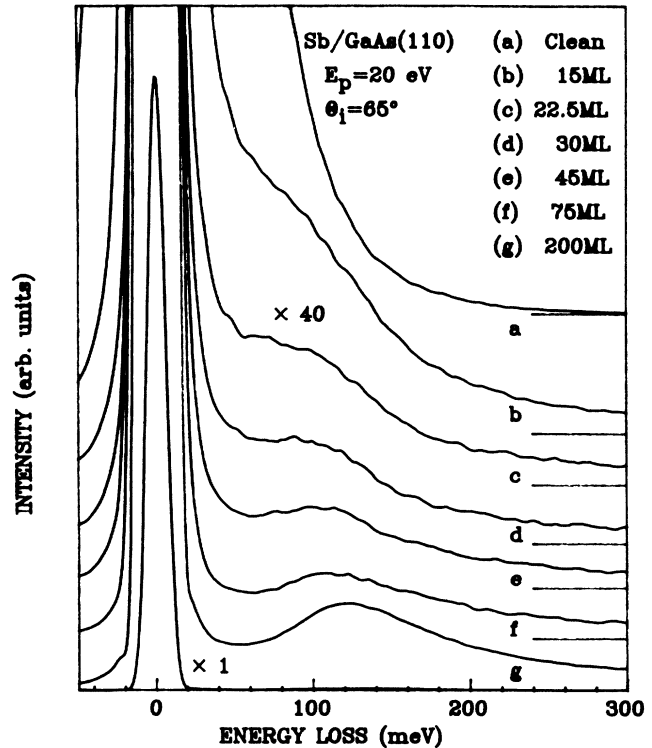


FIG. 12. High-resolution electron-energy-loss spectra of the Sb/[*n*-type GaAs(110)] system, as a function of the Sb coverage, in the low-energy electronic excitation region. Primary beam energy  $E_p = 20$  eV; angle of incidence  $\theta_i \approx 65^\circ$ ; doping concentration  $n \sim 10^{17}$  cm<sup>-3</sup>. Spectra are normalized to the respective elastic-peak areas.

#### D. Low-energy electronic transition region

We took HREELS data in the band-gap-energy region of GaAs, at Sb coverages of 1.2 and 12 ML. At  $\Theta \approx 1.2$  ML there was no evidence of states up to about 1.4 eV of loss energy (we had a HREELS signal of 2 counts/s over an elastic-peak intensity of 170 000 counts/s). At  $\Theta \approx 12$  ML as well we had an average signal of 20 counts/s over an elastic-peak intensity of 150 000 counts/s. The possible presence of electronic states would have been below the detection limit of the HREELS technique. The average structureless signal was indeed below 0.01% of the elastic-peak height in that energy-loss region. On the other hand, as a loss structure appeared at 0.1 eV for  $\Theta > 15$  ML, it had an intensity of the order of 0.4% of the elastic-peak intensity. Interface states located in the band gap were found very recently in a theoretical calculation,<sup>22</sup> for the submonolayer coverages. They would arise from the incomplete bonding of the Sb atoms to the substrate. We have no data in this energy region for the submonolayer coverages, but we can surely rule out the presence of such interface states for the coverages of 1.2 and 12 ML.

At the coverage of 15 ML, a structure appears at about 90 meV of loss energy (Fig. 12). At lower Sb thickness we have no evidence of such a structure, although we cannot

completely excluded its presence, since the high-energy tail of the Fuchs-Kliwer phonon is still very intense. As the Sb coverage increases, this structure shifts to higher energies continuously, reaching an energy of about 125 meV for  $\Theta \approx 200$  ML. As we showed in a previous work,<sup>38</sup> this mode is equivalent to that found for a 0.3- $\mu\text{m}$ -thick Sb layer deposited onto a sputtered GaAs(110) surface. The shape and intensity (0.4% of the elastic-peak intensity) of this feature are those typical of an electronic transition. Crystalline antimony is a semimetal and the Fermi level crosses the conduction band in some points of the Brillouin zone (BZ). A few points of the BZ present energy gaps. Assuming that a relatively high joint density of states (JDOS) is present at these points of the BZ, electronic excitations can indeed be observed across the gaps, superimposed on the continuum of intraband transitions typical of the semimetal. Pseudopotential calculations<sup>44</sup> of the electronic structure of antimony found an electronic minimum located at point *L* of the BZ, opening a gap of about 0.1–0.2 eV, as well as a direct energy gap of the same order of magnitude at point *H*. Band-structure calculations for bulk antimony are available, either with no consideration of the spin-orbit interaction<sup>45</sup> or with consideration of the relativistic approach.<sup>46</sup> In the latter calculation, the maximum of the valence band of Sb was found at point *H* of the BZ and an energy gap of 166 meV was estimated. A gap of similar magnitude was also found in very recent surface band-structure calculations<sup>47</sup> performed with a tight-binding method for the (111) surface of Sb. This gap opens between two bands of non-spin-degenerate surface states arising in the gap between the conduction and valence bands.

Hence, although we cannot yet establish whether the observed transition is related more to surface than to bulk band states, we can undoubtedly attribute the loss feature at about 0.1 eV to an electronic transition between bands characteristic of antimony. From the experimental point of view, a confirmation of this attribution comes from previous magneto-optical experiments on single-crystal Sb specimens, where an average energy gap of 0.1 eV was estimated.<sup>48</sup>

A question arises regarding the explanation of the evolution (changes in position and shape) of this electronic transition loss structure, upon increasing the Sb coverage; namely, whether it is due to an interaction of the overlayer states with the substrate electronic states, or to a “size effect” determined by the increasing overlayer thickness. In the following subsection we shall deal with this problem.

#### E. Model loss function and comparison with the experimental loss function

We recall briefly that—in a HREELS experiment—the differential electron scattering excitation cross section, in the dipolar approximation, can be expressed as the scattering efficiency calculated by Mills.<sup>32</sup> Within certain approximations it can be factorized into two terms: the kinematic prefactor and the loss function, the last factor being proportional to the inverse of the imagi-

nary part of the complex dielectric function. Thus, it is possible to obtain from the experimental loss function the complex dielectric function of a system.

In order to analyze the evolution of the electronic-transition-related loss feature at 0.1 eV, as a function of Sb coverage, we extracted the experimental loss function (LF) from the HREELS data at each coverage step. Thereafter, we compared each LF with the corresponding calculated model LF that we calculated by applying the three-layer model<sup>32</sup> (vacuum-overlayer-substrate) to our system in the 45–500-meV energy-loss range, where the electronic transition structure was found. Within the three-layer model an effective dielectric function  $\bar{\epsilon}$  was constructed as a function of the substrate [ $\epsilon_{\text{GaAs}}(\omega)$ ] and overlayer [ $\epsilon_{\text{Sb}}(\omega)$ ] complex dielectric functions, as well as a function of the overlayer thickness (*d*).

To calculate the model LF's we needed as ingredients the substrate and the overlayer complex dielectric functions, considering the overlayer thickness as a parameter. We proceeded as follows. First, we determined the experimental LF of antimony, and then derived from it the Sb complex dielectric function (through Kramers-Kronig analysis<sup>49</sup>). We then inserted  $\epsilon_{\text{Sb}}(\omega)$  and  $\epsilon_{\text{GaAs}}(\omega)$  (the latter taken from the literature<sup>50</sup>) into the model and calculated the model LF's as a function of the thickness *d*. Finally, we compared them with the experimental ones.

We used the spectrum relative to a coverage of 200 ML to get the LF of Sb. First, we subtracted a background curve from the HREELS spectrum. This curve was evaluated by fitting the elastic and phonon peaks (the major structures in the low-energy region) with Gaussian curves. The background subtraction was done to avoid the influence of the high-energy tail of the phonon peak

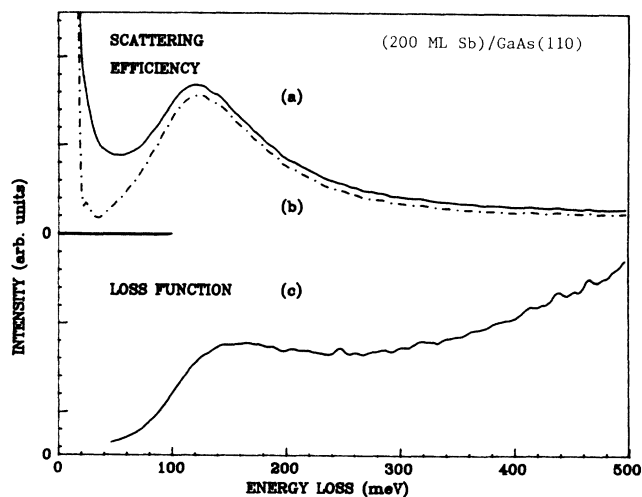


FIG. 13. (a) Energy-loss spectrum (scattering efficiency) of the low-energy excitation region of Sb in the Sb/GaAs(110) system, for a coverage of 200 ML; (b) the same after background subtraction; (c) the corresponding loss function obtained after the kinematic prefactor division.

on the electronic transition structure (we recall that this latter feature was indeed much less intense than the vibrational loss). After the background subtraction, we divided the data (scattering efficiency) by the appropriate kinematic prefactor (obtained after integration with a Gaussian weight over the angular aperture of the analyzer entrance slit<sup>37</sup>). The loss function relative to Sb, shown in Fig. 13, is the result of this procedure.

Knowing the LF of antimony, a second step was the derivation of its complex dielectric function. To do this it was necessary to know the Sb LF in a wide energy range and to know its absolute value.<sup>49</sup> We overcame these difficulties by (a) connecting our LF to that derived from optical measurements by Cardona and Greenaway,<sup>51</sup> in the 1–20-eV energy range, and (b) using a linear and a cubic extrapolation of the LF to low and high energies, respectively.<sup>49</sup> A linear link was used between our LF and that by Cardona and Greenaway,<sup>51</sup> in the 0.5–1-eV energy region. We chose the linear link in such a way as to avoid discontinuities in the derivative of the whole curve. This also established a reasonable normalization factor for our LF.

Having obtained the LF in an energy region comprising all the main structures of antimony, satisfying the sum rules, we analyzed it by means of a Kramers-Kronig procedure<sup>49</sup> and finally obtained the real [ $\epsilon_1(\omega)$ ] and imaginary [ $\epsilon_2(\omega)$ ] parts of the complex dielectric function of Sb in the 0–1-eV energy region, as shown in Fig. 14. A maximum is present in  $\epsilon_2(\omega)$  at about 240 meV, corresponding to a zero of the  $\epsilon_1(\omega)$ . This maximum is superimposed on a strongly decreasing curve, whose slope is very high at low energies, clear indication of metallic behavior. Thus, the maximum in  $\epsilon_2(\omega)$  is clearly related to the 125-meV LF structure, even if the very-low-energy intraband transitions shift it to 240 meV. The complex dielectric function we obtained for Sb has a close similarity with that measured for Bi,<sup>52</sup> which shows a maximum at 700 meV, superimposed on a decreasing curve. The maximum in  $\epsilon_2(\omega)$  of Bi corresponds to an electronic transition analogous to that of antimony, these elements both being semimetals and both presenting energy gaps at a few points of the BZ, with slightly different values.<sup>45,46</sup>

We finally put the obtained  $\epsilon_{Sb}(\omega)$ , together with the  $\epsilon_{GaAs}(\omega)$  taken from the literature,<sup>50</sup> into the three-layer model and built up the model LF's, parametrized by the overlayer thickness  $d$ . The model LF's calculated as a function of  $d$  are shown in Fig. 15, compared with the corresponding experimental LF's. The very good agreement at the higher coverages is a sign of the reliability of the method we used. At the intermediate and low coverages (from 30 to 15 ML), the agreement is still good. In particular, the energy shift—from 125 to 165 meV—of the maximum of the experimental LF found as  $d$  increases from 15 to 200 ML is very well reproduced. Moreover, a "smoothing" of the triangular shape of the experimental LF—upon increasing  $d$ —is also very well reproduced by the model calculation. Small discrepancies are present only in the high-energy tail of the curves, probably due to the background subtraction and normalization procedures. Nevertheless, these discrepancies do

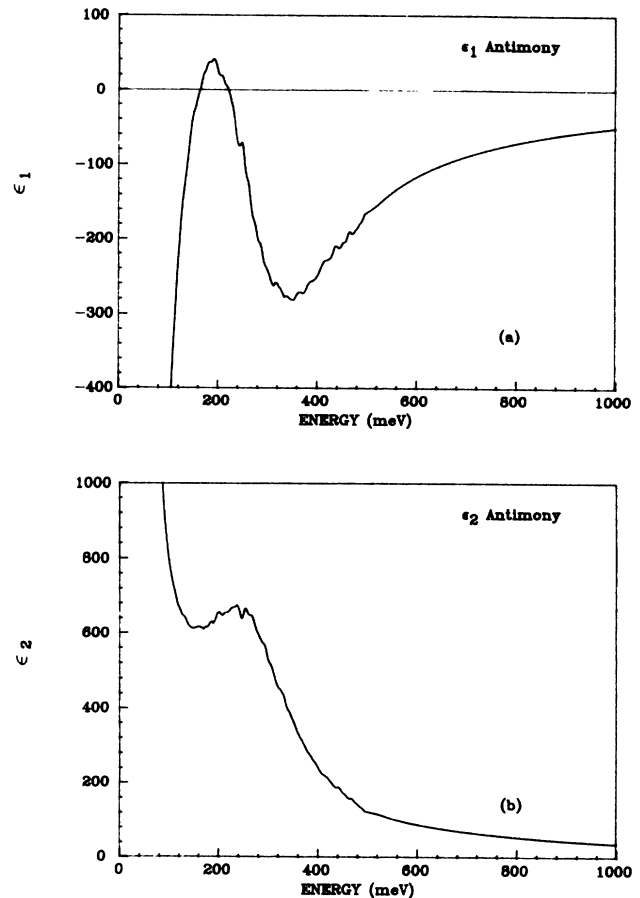


FIG. 14. Imaginary [ $\epsilon_2(\omega)$ ] and real [ $\epsilon_1(\omega)$ ] parts of the complex dielectric function of Sb, in the 45–500-meV energy range.

not affect the main physical information on the feature between 100 and 300 meV.

In conclusion, very good agreement was found between the experimental LF's of the Sb/GaAs(110) system and those calculated through a layer model, in the 0.045–0.5-eV energy-loss range for the various overlayer thickness exploited. Thus, "size effects" of the increasing overlayer thickness are certainly responsible for the changes observed in the spectral characteristics of the structure at about 0.1 eV, upon increasing the coverage. Its energy shift and shape modification are essentially caused by the influence that the boarder conditions of the overlayer have on the electronic structure of antimony.

#### IV. CONCLUSIONS

A HREELS experiment on the Sb/[*n*-type GaAs(110)] system grown at room temperature and in a very wide coverage range was presented. We examined different energy-loss regions corresponding to the quasielastic peak, the Fuchs-Kliwer optical phonon of GaAs, the dopant-free-carrier-induced plasmon, and the low-energy electronic transition region. The analysis of the intensity

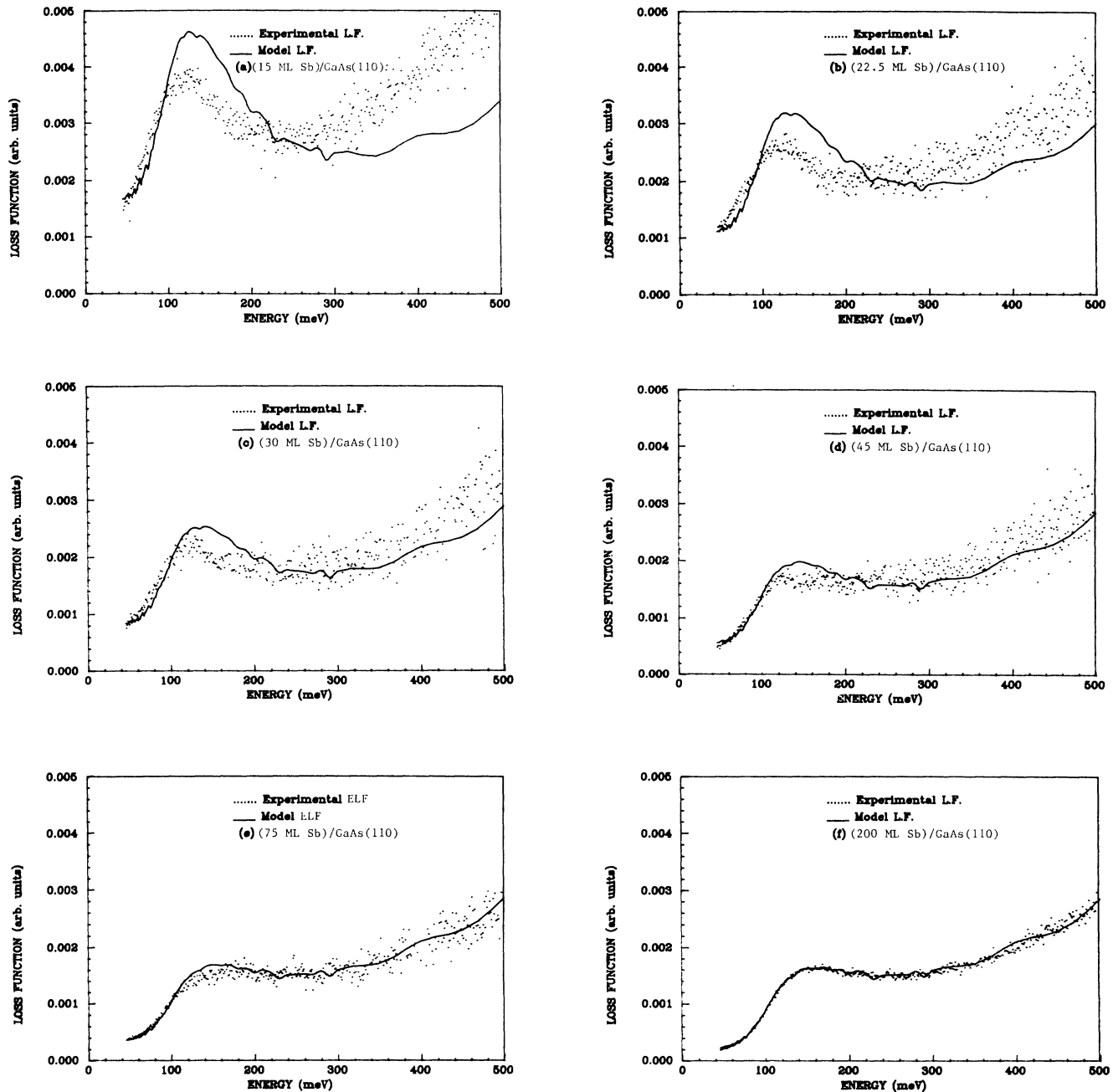


FIG. 15. Comparison of the experimental loss functions (dotted lines) with the calculated model loss functions (solid lines) of the Sb/GaAs(110) system at various stages of antimony coverage.

and position of the Fuchs-Kliwer phonon showed the presence of a critical coverage of 15 ML. At this thickness, antimony undergoes an amorphous-polycrystalline transition as well as a semiconductor-semimetal transition. The screening properties characteristic of these two phases of the overlayer were reflected in the intensity of the quasielastic peak, of the phonon, and of the plasmon. The modification of the plasmon energy, as a function of coverage, was related to the change in the space-charge-layer depth and to the band bending at the interface be-

tween Sb and GaAs. The presence of states of different origin inducing the band bending (defect induced at the low coverages, electron interface states at the higher) has been suggested.

Through analysis of the HREELS data the complex dielectric function of Sb in the 0.045–0.5-eV energy region was obtained for the first time, to our knowledge.

A loss structure, which we had already attributed<sup>38</sup> to an electronic transition characteristic of antimony, was analyzed at the different coverage steps. An energy shift

and a shape modification of this feature were observed. We derived the experimental loss functions from the data and compared them with those obtained by means of a layer-model calculation. The good agreement found allowed us to explain the energy and shape modifications of this structure as due to "size effects" induced by the increasing overlayer thickness.

Finally, we believe that this research demonstrates the very high versatility of the HREELS technique in studying several physical aspects of surface and interface systems, such as their vibrational and electronic structure. HREELS has also been shown to be an extremely powerful technique for identifying and characterizing narrow-

gap surface systems. Extension of this kind of investigation to other semimetal-III-V-semiconductor systems will surely give a better understanding of such interfaces, especially at higher coverages.

#### ACKNOWLEDGMENTS

The experimental assistance provided by E. Angeli is gratefully acknowledged. Data analysis was performed at the computer center of the Università degli Studi di Modena. Financial support of this research came from the European Community, through Grant No. ST2J-0333-C.

\*Present address: Istituto di Struttura della Materia, Consiglio Nazionale delle Ricerche, via Enrico Fermi 38, I-00044 Frascati (Roma), Italy.

<sup>1</sup>P. Skeath, C. Y. Su, I. Lindau, and W. E. Spicer, *J. Vac. Sci. Technol.* **17**, 874 (1980).

<sup>2</sup>P. Skeath, I. Lindau, C. Y. Su, and W. E. Spicer, *J. Vac. Sci. Technol.* **19**, 556 (1981).

<sup>3</sup>J. Carelli and A. Kahn, *Surf. Sci.* **116**, 380 (1982).

<sup>4</sup>C. B. Duke, A. Paton, W. K. Ford, A. Kahn, and J. Carelli, *Phys. Rev. B* **26**, 803 (1982).

<sup>5</sup>C. M. Bertoni, C. Calandra, F. Manghi, and E. Molinari, *Phys. Rev. B* **27**, 1251 (1983).

<sup>6</sup>Zhang Kai-Ming and Xu Yong-Nian, *J. Vac. Sci. Technol. B* **1**, 729 (1983).

<sup>7</sup>C. Mailhot, C. B. Duke, and D. J. Chadi, *Phys. Rev. B* **31**, 2213 (1985).

<sup>8</sup>M. Mattern-Klosson and H. Lüth, *Solid State Commun.* **56**, 1001 (1985).

<sup>9</sup>L. Li and A. Kahn, *J. Vac. Sci. Technol. A* **4**, 358 (1986).

<sup>10</sup>A. Tulke, M. Mattern-Klosson, and H. Lüth, *Solid State Commun.* **59**, 303 (1986).

<sup>11</sup>A. Tulke and H. Lüth, *Surf. Sci.* **178**, 131 (1986).

<sup>12</sup>P. Mårtensson, G. V. Hansson, M. Lähdeniemi, R. O. Magnusson, S. Wiklund, and J. M. Nicholls, *Phys. Rev. B* **33**, 7399 (1986).

<sup>13</sup>M. Mattern-Klosson, R. Strümpfer, and H. Lüth, *Phys. Rev. B* **33**, 2559 (1986).

<sup>14</sup>W. Pletschen, N. Esser, H. Mündler, D. Zahn, J. Geurts, and W. Richter, *Surf. Sci.* **178**, 140 (1986).

<sup>15</sup>M. Hünermann, W. Pletschen, U. Resch, U. Rettweiler, W. Richter, J. Geurts, and P. Lautenschlager, *Surf. Sci.* **189/190**, 322 (1987).

<sup>16</sup>D. E. Savage and M. G. Lagally, *Appl. Phys. Lett.* **50**, 1719 (1987).

<sup>17</sup>R. Strümpfer and H. Lüth, *Surf. Sci.* **182**, 545 (1987).

<sup>18</sup>F. Schäffler, R. Ludeke, A. Taleb-Ibrahimi, G. Hughes, and D. A. Rieger, *Phys. Rev. B* **36**, 1328 (1987); *J. Vac. Sci. Technol. B* **5**, 1048 (1987).

<sup>19</sup>W. Drube, F. J. Himpsel, and R. Ludeke, *J. Vac. Sci. Technol. B* **5**, 930 (1987); W. Drube and F. J. Himpsel, *Phys. Rev. B* **37**, 855 (1988).

<sup>20</sup>R. Cao, K. Myiano, T. Kendelewicz, I. Lindau, and W. E. Spicer, *Surf. Sci.* **206**, 413 (1988); Renyu Cao, K. Myiano, I. Lindau, and W. E. Spicer, *J. Vac. Sci. Technol. A* **7**, 738 (1989).

<sup>21</sup>R. M. Feenstra and P. Mårtensson, *Phys. Rev. Lett.* **61**, 447

(1988); P. Mårtensson and R. M. Feenstra, *Phys. Rev. B* **39**, 7744 (1989).

<sup>22</sup>F. Manghi and C. Calandra, in *Proceedings of the 7th International Conference on Solid Surfaces, Köln (1989)* [Vacuum (to be published)].

<sup>23</sup>R. I. Sharp and E. Warming, *J. Phys. F* **1**, 570 (1971).

<sup>24</sup>J. S. Lannin, J. M. Calleja, and M. Cardona, *Phys. Rev. B* **12**, 585 (1975).

<sup>25</sup>Jeffrey S. Lannin, *Phys. Rev. B* **15**, 3863 (1977).

<sup>26</sup>T. S. Moss, in *Photoconductivity in the Elements* (Butterworths, London, 1952).

<sup>27</sup>L. Ley, R. A. Pollak, S. P. Kowalczyk, R. McFeely, and D. A. Shirley, *Phys. Rev. B* **8**, 641 (1973).

<sup>28</sup>G. N. Greaves, E. A. Davis, and J. Bordas, *Philos. Mag.* **34**, 265 (1976).

<sup>29</sup>J. Knights, *Solid State Commun.* **16**, 515 (1975); J. C. Knights and J. E. Mahan, *ibid.* **21**, 983 (1977).

<sup>30</sup>C. Raisin, G. Leveque, and S. Robin-Kandare, *J. Phys. C* **9**, 2887 (1976).

<sup>31</sup>C. Raisin, G. Leveque and S. Robin, *Solid State Commun.* **14**, 723 (1974).

<sup>32</sup>D. L. Mills, *Surf. Sci.* **48**, 59 (1975); H. Ibach and D. L. Mills, *Electron Energy Loss Spectroscopy and Surface Vibrations* (Academic, New York, 1982).

<sup>33</sup>R. Matz and H. Lüth, *Phys. Rev. Lett.* **46**, 500 (1981).

<sup>34</sup>Maria Grazia Betti, U. del Pennino, and Carlo Mariani, *Phys. Rev. B* **39**, 5587 (1989); Y. Chen, S. Nannarone, J. Schaefer, J. C. Hermanson, and G. J. Lapeyre, *ibid.* **39**, 7653 (1989).

<sup>35</sup>H. Froitzheim and H. Ibach, *Surf. Sci.* **47**, 713 (1975); U. del Pennino, Maria Grazia Betti, Carlo Mariani, and I. Abbati, *ibid.* **207**, 133 (1988).

<sup>36</sup>S. R. Streight and D. L. Mills, *Phys. Rev. B* **38**, 8526 (1988).

<sup>37</sup>U. del Pennino, M. G. Betti, C. Mariani, C. M. Bertoni, S. Nannarone, I. Abbati, L. Braicovich, and A. Rizzi, *Solid State Commun.* **60**, 337 (1986); U. del Pennino, M. G. Betti, C. Mariani, C. M. Bertoni, S. Nannarone, I. Abbati, L. Braicovich, and A. Rizzi, *Surf. Sci.* **189/190**, 689 (1987).

<sup>38</sup>Carlo Mariani, Maria Grazia Betti, and U. del Pennino, *Phys. Rev. B* **40**, 8095 (1989).

<sup>39</sup>J. J. Yeh and I. Lindau, *At. Data Nucl. Data Tables* **32**, 1 (1985).

<sup>40</sup>L. H. Dubois, G. P. Schwartz, R. E. Camley, and D. L. Mills, *Phys. Rev. B* **29**, 3208 (1984).

<sup>41</sup>A. Pinczuk, G. Abstreiter, R. Trommer, and M. Cardona, *Solid State Commun.* **21**, 959 (1977); Takeshi Inaoka and Takeshi Chihara, *Surf. Sci.* **208**, 71 (1989); Takeshi Inaoka (un-

- published).
- <sup>42</sup>D. H. Ehlert and D. L. Mills, *Phys. Rev. B* **36**, 1051 (1987); **34**, 3939 (1986).
- <sup>43</sup>Y. Chen, G. J. Lapeyre, and Y. Xu, *J. Vac. Sci. Technol. A* **6**, 686 (1988).
- <sup>44</sup>L. M. Falikov and P. J. Lin, *Phys. Rev.* **141**, 562 (1966); L. A. Fal'kovskii, *Fiz. Tverd. Tela (Leningrad)* **28**, 270 (1986) [*Sov. Phys.—Solid State* **28**, 146 (1986)].
- <sup>45</sup>John Robertson, *Phys. Rev. B* **28**, 4671 (1983).
- <sup>46</sup>J. Rose and R. Schuchardt, *Phys. Status Solidi B* **139**, 499 (1987).
- <sup>47</sup>S. N. Molotkov and V. V. Tatarsky, *Acad. Sci. U.S.S.R., Surf. Phys. Chem. Mech.* **5**, 17 (1988).
- <sup>48</sup>Mildred S. Dresselhaus and John G. Mavroides, *Solid State Commun.* **2**, 297 (1964); *Phys. Rev. Lett.* **14**, 259 (1965).
- <sup>49</sup>J. Daniels, C. v. Festenberg, H. Raether, and K. Zeppenfelds, in *Optical Constants of Solids by Electron Spectroscopy*, Vol. 54 of *Springer Tracts in Modern Physics*, edited by G. Höhler (Springer-Verlag, Berlin, 1970), p. 77.
- <sup>50</sup>E. D. Palik, *Handbook of Optical Constants* (Academic, New York, 1985).
- <sup>51</sup>Manuel Cardona and D. L. Greenaway, *Phys. Rev.* **133**, A1685 (1964).
- <sup>52</sup>J. Hageman, W. Gudat, and C. Kunz, DESY Internal Report No. SR-74/7, 1974 (unpublished).